

MEASUREMENT OF TWO- AND FOUR-PARTICLE CORRELATIONS IN P-PB AND PB-PB COLLISIONS AT CMS *

Jovan Z. Milošević
on behalf of the CMS Collaboration

Abstract. Results of two- and four-particle angular two-dimensional correlations in pPb collisions at a nucleon-nucleon center-of-mass energy of 5.02 TeV, collected with the CMS detector, are presented. In high-multiplicity pPb events a ridge-like structure at the near-side emerges in two-particle $\Delta\eta - \Delta\phi$ correlation. It is compared to the ridge found in 2.76 TeV PbPb collisions. In both systems, the ridge yield rises, reaches a maximum at $p_T \approx 1 - 3$ GeV/c and then decreases at higher p_T , and increases monotonically with multiplicity. The 2-nd order Fourier harmonic has qualitatively similar p_T dependence, but with a moderate multiplicity dependence in both systems. The multiplicity dependence of the 3-rd Fourier harmonic is rather similar for pPb and PbPb collisions. Color glass condensate and hydrodynamic predictions are compared to the experimental results.

1. Introduction

Two- and multi-particle correlations are promising tool to study collective phenomena in high energy protons and nuclei collisions. Correlating particles in $\Delta\phi$ and $\Delta\eta$ ¹ a reach structure emerges. The finding of the ridge structure in both PbPb [1] and pPb [2] CMS data attracted a lot of attention. A most pronounced source of the composite signal originate from the second Fourier component, called 'elliptic flow'. The third Fourier component, the triangular flow, appears to be a significant source of the overall signal too. Recently, a similar long-range ($|\Delta\eta| > 2$) correlation has been found in smallest pp system [3] with very high multiplicity. Usually hydrodynamics is used to explain seen phenomena in large nucleus-nucleus collision system, while different theoretical models are trying to explain it for the small systems formed in pp or pPb collisions.

Received June 20, 2014.

UDC 539.12

*The author has been supported in by Ministry of Education, Science and Technological Development of Republic of Serbia within the Project 171019

¹ $\Delta\phi$ and $\Delta\eta$ are differences in azimuthal angle ϕ and pseudorapidity $\eta = -\ln(\tan(\theta/2))$ between particles in a pair

2. Experiment

The Compact Muon Solenoid (CMS) experiment is a general-purpose particle detector at the Large Hadron Collider (LHC) at CERN. It has a cylindrical layered subdetector structure with huge dimensions: 25 m long, 15 m in diameter and its weight is about 12500 tons. The innermost layer is silicon tracker. It is surrounded with electromagnetic and then with hadronic calorimeter. All of them are inside the CMS solenoid which produces 3.8 T magnetic field. Muon chambers are placed outside the magnet. As the detector covers full azimuthal angle and a large pseudo-rapidity range it is well suited for the correlation studies. A more detailed description of the CMS detector can be found in [4]. The main results in the analysis presented here are obtained using the silicon tracker.

2.1. Experimental data

The LHC pPb run at the beginning of 2013 provided data used in this analysis. These data were collected by CMS detector. Protons with 4 TeV energy have been collided with Pb nuclei accelerated to 1.58 A TeV resulting in a nucleon-nucleon center-of-mass energy of 5.02 TeV. The PbPb data at $\sqrt{s_{NN}}=2.76$ TeV, used here for comparison, have been recorded during 2011.

The analysed pPb events were divided into several centrality classes based on number of reconstructed tracks, $N_{trk}^{offline}$. Only tracks with $|\eta| < 2.4$ and $p_T > 0.4$ GeV/c were counted. Details on the criteria applied on track selection are described in [5].

3. Methodology

3.1. Two-particle correlation function

The two-particle correlation is built by pairing 'trigger' and 'associated' particle. The trigger (associated) particle is defined as charged primary particle within a given p_T^{trig} (p_T^{assoc}) range. With N_{trig} is denoted the number of trigger particles in the event. For each centrality, *i.e.* track multiplicity class, the per-trigger particle associated yield is defined as

$$(3.1) \quad \frac{1}{N_{trig}} \frac{d^2 N^{pair}}{d\Delta\eta d\Delta\phi} = B(0,0) \frac{S(\Delta\eta, \Delta\phi)}{B(\Delta\eta, \Delta\phi)}$$

The signal distribution, normalized by N_{trig} ,

$$(3.2) \quad S(\Delta\eta, \Delta\phi) = \frac{1}{N_{trig}} \frac{d^2 N^{same}}{d\Delta\eta d\Delta\phi}$$

is constructed by pairing particles within the same event, while the normalized background distribution

$$(3.3) \quad B(\Delta\eta, \Delta\phi) = \frac{1}{N_{trig}} \frac{d^2 N^{mix}}{d\Delta\eta d\Delta\phi}$$

²which could be either the same or different from the p_T^{trig} range

is obtained by forming pairs where the trigger particle is taken from one event while associated particles are taken from another event. In order to reduce statistical errors which comes from the background, the event mixing procedure is repeated 10 times by choosing different, but topologically similar events. The normalization of the correlation function is achieved by factor $B(0,0)$ in (3.1) which represents mixed-event associated yield around zero³.

3.2. Fourier harmonics from two- and four-particle correlations

For a given $(p_T^{trig}, p_T^{assoc})$ bin, the azimuthal anisotropy harmonics, $V_{n\Delta}$, are obtained from a Fourier decomposition of long-range two-particle $\Delta\phi$ correlation function

$$(3.4) \quad \frac{1}{N_{trig}} \frac{dN^{pair}}{d\Delta\phi} = \frac{N_{assoc}}{2\pi} \left\{ 1 + \sum_n 2V_{n\Delta} \cos(n\Delta\phi) \right\}$$

In Fourier decomposition (3.4) the first three harmonics are included. Inclusion of higher harmonics gave negligible effects on the Fourier fit. The long-range correlation is obtained by applying an η gap of 2 units in order to remove short-range correlations which comes from jet fragmentation. Using the fitted Fourier harmonics $V_{n\Delta}$, the elliptic and triangular flow harmonics are extracted as

$$(3.5) \quad v_n\{2, |\Delta\eta| > 2\}(p_T) = \frac{V_{n\Delta}(p_T, p_T^{ref})}{\sqrt{V_{n\Delta}(p_T^{ref}, p_T^{ref})}}, n = 2, 3$$

The p_T range for the 'reference' particle is $0.3 < p_T < 3.0$ GeV/c.

Beside the two-particle correlations, the Q-cumulant method [7] based on four-particle correlations have been also used to extract the elliptic flow. First, one calculates the reference value

$$(3.6) \quad v_2^{ref}\{4\} = \sqrt[4]{-c_2\{4\}}$$

where four-particle cumulant $c_2\{4\}$ is obtained as

$$(3.7) \quad c_2\{4\} = \langle\langle e^{in(\phi_1+\phi_2-\phi_3-\phi_4)} \rangle\rangle - 2\langle\langle e^{in(\phi_1-\phi_2)} \rangle\rangle$$

In (3.7), $\phi_i, i = 1, \dots, 4$ are azimuthal angles of four corresponding particles in a given event while $\langle\langle \rangle\rangle$ denotes an averaging over all particles and over all events in an analyzed multiplicity range. Once, having reference elliptic flow determined by (3.6) the differential elliptic flow is given by

$$(3.8) \quad v_2\{4\}(p_T) = \frac{-d_2\{4\}(p_T)}{(v_2^{ref}\{4\})^3}$$

With $d_2\{4\}(p_T)$ is denoted differential four-particle cumulant which is obtained using (3.7) with a requirement that one of four particles belongs to the given p_T interval. As the four-particle cumulant method, by itself suppresses short-range correlation, an explicit η gap requirement was not applied.

³The bin width of 0.3 in $\Delta\eta$ and $\pi/16$ in $\Delta\phi$ is used

4. Results

2-D two-particle correlation functions constructed in PbPb collisions at $\sqrt{s_{NN}} = 2.76 \text{ TeV}$ (left) and pPb collisions at $\sqrt{s_{NN}} = 5.02 \text{ TeV}$ (right) are shown in Fig. 4.1. In these particular figures, the correlations are calculated for charged particle pairs with $1 < p_T^{assoc}, p_T^{trig} < 3 \text{ GeV}/c$ and within multiplicity range $220 < N_{trk}^{offline} < 260$. In order to better illustrate correlation structure the correlation

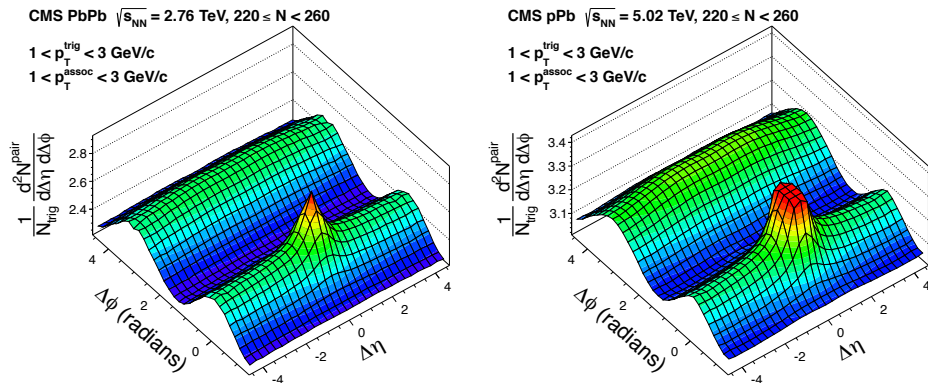


FIG. 4.1: 2-D two-particle correlations in $\Delta\phi$ and in $\Delta\eta$ for PbPb collisions at $\sqrt{s_{NN}} = 2.76 \text{ TeV}$ (left) and pPb collisions at $\sqrt{s_{NN}} = 5.02 \text{ TeV}$ (right). They are constructed within multiplicity range $220 < N_{trk}^{offline} < 260$ for fixed p_T^{assoc} and p_T^{trig} intervals. In order to emphasize the structure, the near-side peak from the jet fragmentation has been truncated.

peak near $(\Delta\phi, \Delta\eta) = (0, 0)$, which appears due to the jet correlation, is truncated. Beside the jet structure, a strong 'ridge-like' structure at $\Delta\phi \approx 0$ and elongated in $\Delta\eta$ is seen. Earlier, such a structure is seen both in PbPb and in high-multiplicity pp collisions. There is also a long-range structure on the 'away' side ($\Delta\phi \approx \pi$). Together, such a $\cos(2\Delta\phi)$ structure arises mainly due to the elliptic flow in non-central nucleus-nucleus collisions [8].

In order to investigate the seen structure quantitatively we divided it into two regions: 'short-range' and 'long-range' regions which cover $|\Delta\eta| < 1$ and $|\Delta\eta| > 2$ respectively which then were projected onto $\Delta\phi$ axis. The obtained projections are shown in Fig. 4.2 (top panel: PbPb case; bottom panel: pPb case) for the two very distinct multiplicity ranges: $N_{trk}^{offline} < 20$ (open squares) and $220 < N_{trk}^{offline} < 260$ (solid squares) and for five p_T^{trig} interval selections. In both cases p_T interval of associated particles is kept fixed. The lines represent Fourier fit from Eq.(3.4). A similar structure and its evolution with p_T is seen for both PbPb and pPb collisions. In the 'long-range' region, the near side signal has a small variations, while in the 'short-range' region it is opposite. So, the jet fragmentation and 'long-range' correlations contribute to the 'short-range' region, while in the 'long-range'

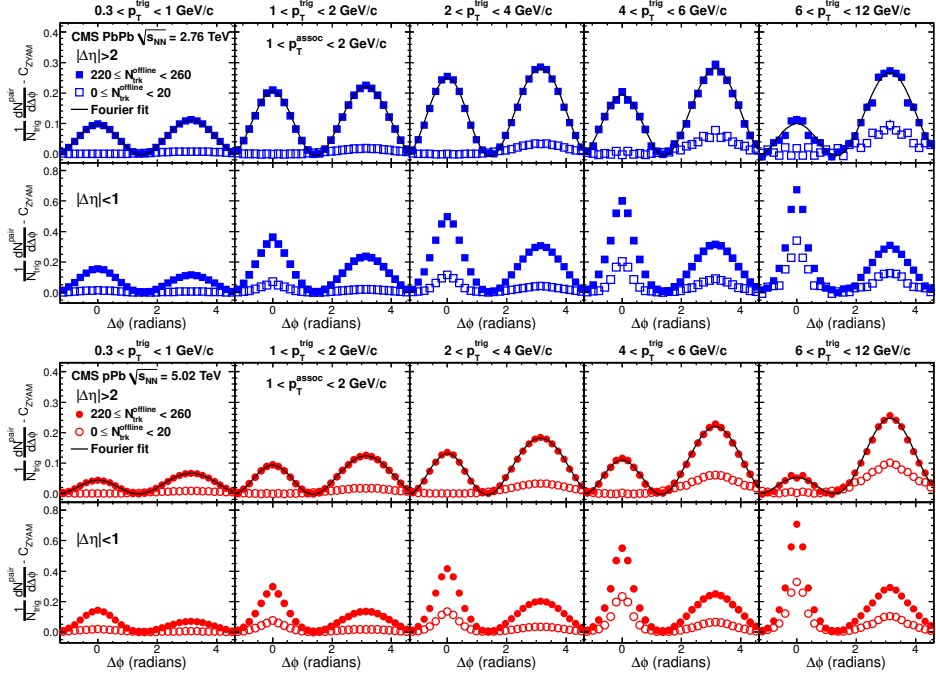


FIG. 4.2: Top panel: 1-D two-particle azimuthal correlations in PbPb collisions at $\sqrt{s_{NN}} = 2.76 \text{ TeV}$ within multiplicity ranges $N_{trk}^{offline} < 20$ (open squares) and $220 < N_{trk}^{offline} < 260$ (solid squares) for a fixed p_T^{assoc} range in five p_T^{trig} ranges. The top (bottom) row corresponds to the long-range (short-range) $|\Delta\eta| > 2.0$ ($|\Delta\eta| < 1.0$) region. Bottom panel: 1-D two-particle azimuthal correlations in pPb collisions at $\sqrt{s_{NN}} = 5.02 \text{ TeV}$ obtained under the same requirements as in the PbPb case

region the jet contribution is significantly suppressed. Practically there are no near-side correlations in the 'long-range' region for both PbPb and pPb low-multiplicity events.

Integrating the associated yield of the near-side ($\Delta\phi < 1.2$) correlations, quantitative comparisons between the 'short' and 'long-range' region could be performed. By subtracting the integrated yield of the 'long-range' region⁴ from the one in the 'short-range' region, the 'jet yield' is obtained. The obtained results are shown in Fig. 4.3 for the high-multiplicity pPb (solid circles) and PbPb (solid squares) events. The ridge yield rises with transverse momentum reaching a maximum at $p_T^{trig} \approx 2 - 3 \text{ GeV}/c$ and then decreases toward zero. The shape of the distributions is similar both in pPb and PbPb collisions, while the magnitude of the ridge yield in PbPb collisions is higher with respect to the one in pPb collisions. On the other side, the jet yield shown in the right part of the Fig. 4.3 increases monotonically

⁴shortly called the 'ridge yield'

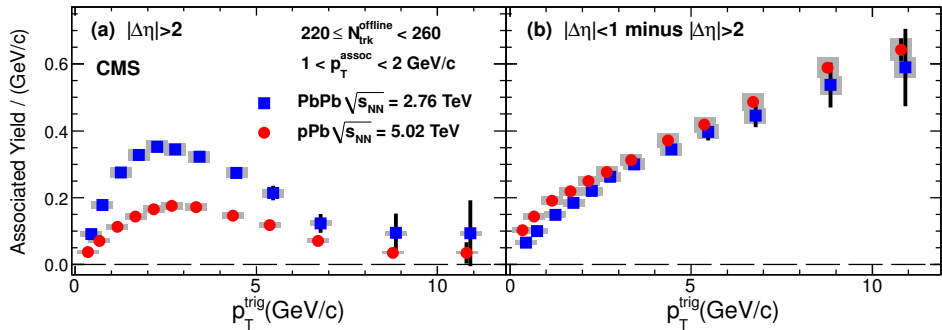


FIG. 4.3: Left (right): The near-side associated yield *vs* p_T^{trig} for the long-range (short-range) region for the multiplicity range of $220 < N_{trk}^{offline} < 260$ in PbPb (solid squares) and pPb (solid circles) collisions. The results for the short-range are obtained after subtraction of the yield from the long-range region.

with p_T and has similar magnitude in both colliding systems. There is a simple explanation for a such behavior: higher jet energy means more particles associated to the jet.

In Fig. 4.4 are shown the ridge (left) and the jet (right) yields in function of multiplicity for the same p_T interval of trigger and associated particles. The ridge yield has a monotonic rise with multiplicity. At a given multiplicity, the ridge yield

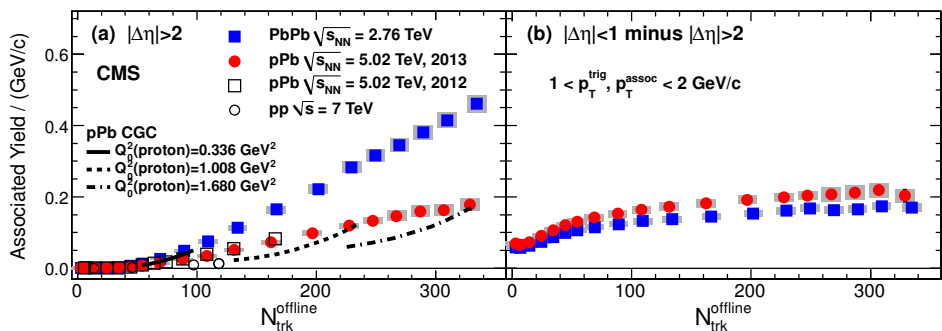


FIG. 4.4: Left (right): The near-side associated yield *vs* $N_{trk}^{offline}$ multiplicity for the long-range (short-range) region .

decreases going from PbPb, trough pPb to the smallest pp system. Similarly to the pp and pPb collisions, the ridge yield in PbPb case achieves non-negligible values for $N_{trk}^{offline} \gtrsim 40 - 50$. In contrast to the ridge yield, the jet yield has a moderate rise with multiplicity. There is a slight, nearly no significant difference in magnitude between the jet yield in PbPb and pPb collisions.

According to the color glass condensate (CGC) model, the ridge-like structure

in pPb collisions is attributed to the initial state gluon correlations. Within that model, the contribution of collimatedly emitted gluons is enlarged in the gluon saturation regime [9, 10, 11]. The model qualitatively describes the data. As the model calculation depends on saturation scales, the CMS data could provide constraints on these parameters in the CGC model.

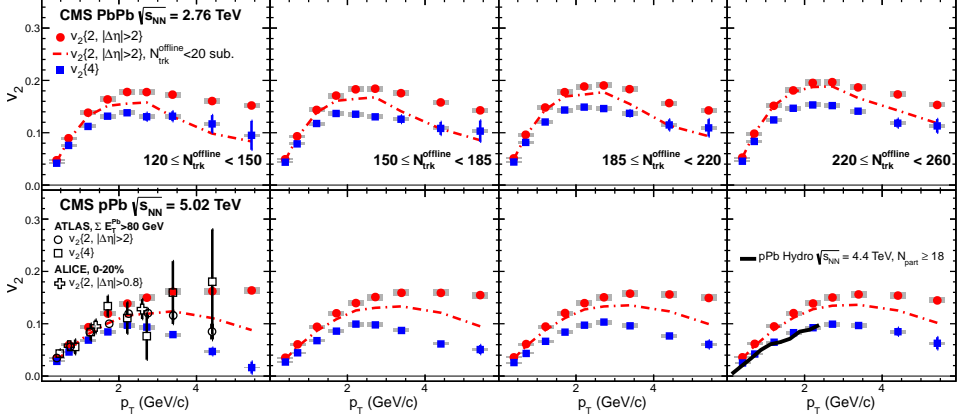


FIG. 4.5: The p_T dependence of the v_2 for four multiplicity ranges in PbPb (top row) and pPb (bottom) collisions. Two- and four-particle correlation techniques are applied to extract the Fourier harmonics. Results after subtracting low-multiplicity data, as well as hydrodynamic predictions are also shown. The open symbols show the results from ALICE [12] and ATLAS [13] experiments.

Another model, relativistic hydrodynamics, also predicts the long-range correlations in pPb collisions [6] as a consequence of a collective movements. In order to compare with hydrodynamic predictions the elliptic (v_2) and triangular (v_3) were calculated from Fourier decomposition of 1-D $\Delta\phi$ correlation functions in the long-range region. The obtained coefficients, in function of p_T , are shown with solid red circles in Fig. 4.5 and 4.6 respectively. In order to reduce non-flow correlations, the v_2 has been additionally extracted using four-particle cumulant method. Hence, this method gives cleaner measurement of collective movements which involves many particles. These results are shown with solid blue squares in Fig. 4.5. The analysis was performed in four multiplicity intervals. The difference between the $v_2\{2, \Delta\eta > 2\}$ and $v_2\{4\}$ could come from event-by-event fluctuations in the flow signal. The magnitude of the v_2 harmonic in PbPb is bigger with respect to the one in pPb collisions. The v_3 harmonic has a smaller magnitude than v_2 . The elliptic and triangular flow shows a similar p_T dependence. The hydrodynamic predictions for the highest analyzed multiplicity interval in pPb data is shown. The hydro calculation describes well the $v_2\{4\}$ although it does not includes the event-by-event fluctuations. The inclusion of these fluctuations would bring the hydro line somewhere between $v_2\{2\}$ and $v_2\{4\}$. Under assumption that the jet correlations does not depend on the event multiplicity in the pPb collisions one can subtract the

results of lowest multiplicity events ($N_{trk}^{offline} \leq 20$) from high-multiplicity events in order to remove the jet contribution. The obtained findings are shown with

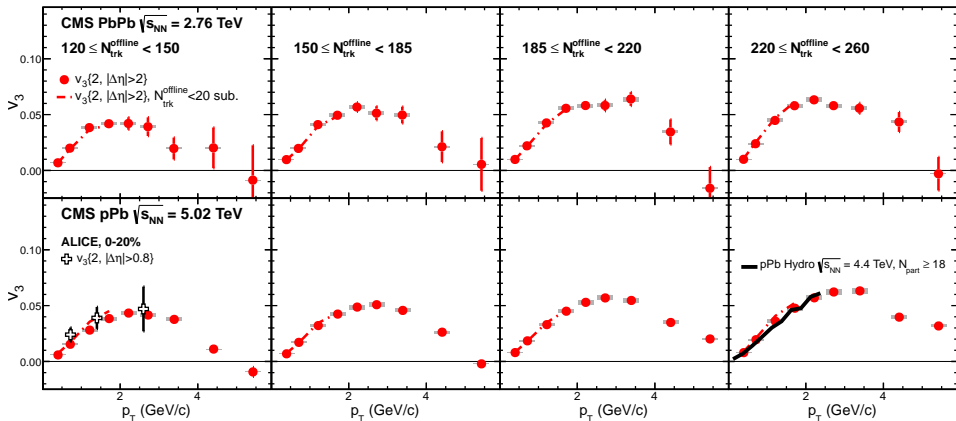


FIG. 4.6: The p_T dependence of the v_3 for four multiplicity ranges in PbPb (top row) and pPb (bottom row) collisions. The same requirements as in Fig. 4.5 are applied here.

dash-dotted lines. At higher p_T this procedure makes v_2 smaller with respect to the $v_2\{2\}$ which is consistent with a stronger jet correlations at higher p_T . The triangular flow remains unchanged under such a subtraction as it can be seen in Fig. 4.6. The CMS results presented in this analysis has much better precision with respect to the ones previously obtained by the ALICE [12] and ATLAS [13] experiments.

Results for the multiplicity dependence of the elliptic and triangular flow in PbPb and pPb collisions, averaged within $0.3 < p_T < 3$ GeV/c, are shown in Fig. 4.7 and 4.8 respectively. In the case of PbPb collisions, the elliptic flow moderately increases with multiplicity, while in the case of pPb collisions it stays relatively constant for larger multiplicities. As it is expected, the magnitude of the v_2 in PbPb collisions is bigger with respect to the one in pPb collisions. This is consistent with the multiplicity dependence of the associated yield shown in Fig. 4.4. The triangular flow, v_3 , has a similar magnitude in both PbPb and pPb collisions. Within the hydrodynamics model such similarity in v_3 is not expected as the initial state geometry is rather different in PbPb and in pPb collisions. The v_3 Fourier coefficient is largely determined by the event-by-event initial state geometry fluctuations. In the low-multiplicity region feasibility of the $v_3\{2\}$ and $v_2\{4\}$ measurements is poor. It could be due to the absence of collective movements in low-multiplicity events or due to the breakdown of four-particle cumulant technique. With dash-dotted lines are shown also the results obtained by applying the procedure of subtracting the low-multiplicity data. These results gives almost the same values as $v_2\{2\}$ in high-multiplicity region which is expected as the jet contribution is suppressed by a factor $1/\sqrt{N_{trk}^{offline}}$. The same procedure does not change the v_3 results at all.

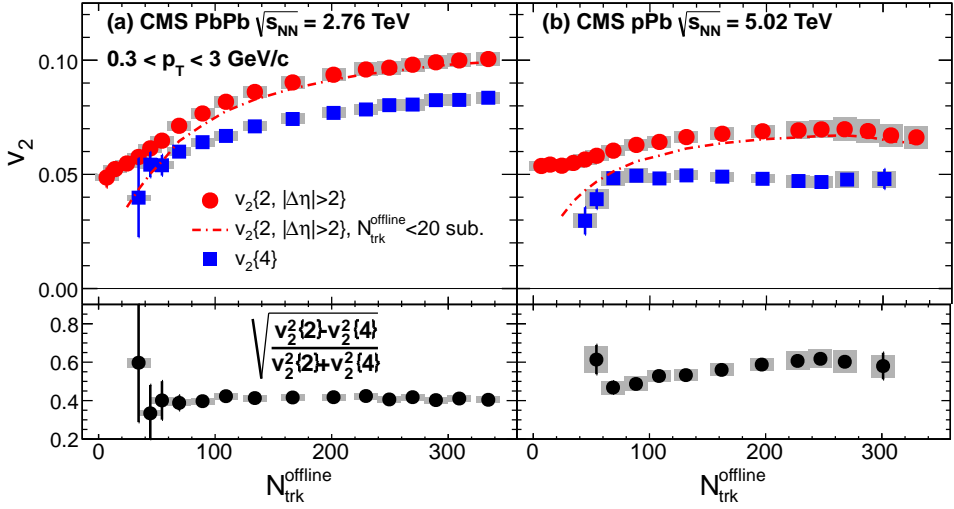


FIG. 4.7: Top: The multiplicity dependence of the v_2 in PbPb (left) and pPb (right) collisions for $0.3 < p_T < 3$ GeV/c. Bottom: The multiplicity dependence of the upper limits on the elliptic flow fluctuations.

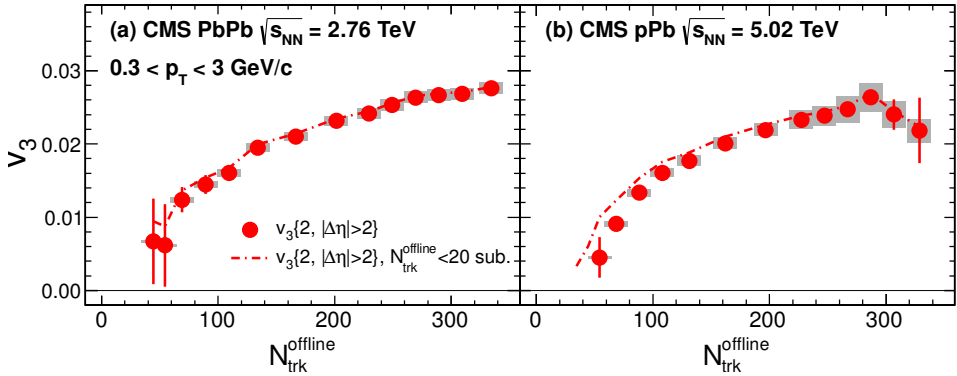


FIG. 4.8: The multiplicity dependence of the v_3 in PbPb (left) and pPb (right) collisions for $0.3 < p_T < 3$ GeV/c.

The variable $\sqrt{(v_2^2\{2\} - v_2^2\{4\})/(v_2^2\{2\} + v_2^2\{4\})}$, used to estimate event-by-event v_2 fluctuations [14], is shown in the bottom panels of Fig. 4.7. In PbPb and pPb collisions are observed fluctuations on the level of 40% and 50-60% respectively which is comparable with the values measured in 200 GeV PbPb collisions at RHIC [15].

In Fig. 4.9, the multiplicity dependence of $v_2\{2\}$ and $v_2\{4\}$, averaged over $0.3 < p_T < 3.0$ GeV/c, from pPb data collected by the CMS experiment are com-

pared with those from the ATLAS experiment⁵. The $v_2\{4\}$ ATLAS results are systematically higher with respect to the CMS data. The seen discrepancy is not large with respect to the errors. Here should be mentioned that the applied cuts on compared ATLAS and CMS data are not precisely the same.

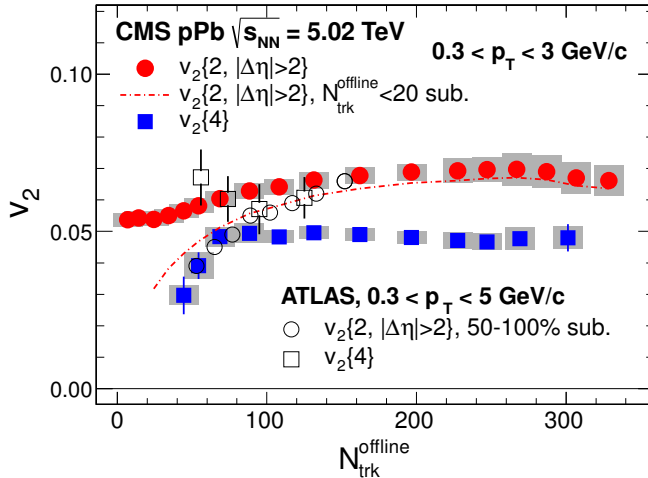


FIG. 4.9: The v_2 measured from two- and four-particle correlations *vs* multiplicity for $0.3 < p_T < 3.0$ GeV/c from pPb data collected by ATLAS (open symbols) and CMS (solid symbols) detector.

5. Summary

Differential analysis of the two- and four-particle correlations is performed on pPb data at $\sqrt{s_{NN}}=5.02$ TeV collected by the CMS detector. A direct comparison between the results from pPb and PbPb is presented as a function of transverse momentum and event multiplicity. The results have been compared with color glass condensate and hydrodynamic predictions as well as with findings from the other experiments. Available statistics which spans over a very broad transverse momentum and particle multiplicity range should provide significant constraints on theoretical predictions of the origin of the long-range ridge phenomena formed in small collision system.

REFERENCES

1. S. CHATRCHYAN *et al.*, CMS Collaboration: *Long-range and short-range dihadron angular correlations in central PbPb collisions at a nucleon-nucleon center of mass energy of 2.76 TeV*. JHEP **1107** (2011), 076.

⁵where results are averaged over the region $0.3 < p_T < 5.0$ GeV/c

2. S. CHATRCHYAN *et al.*, CMS Collaboration: *Observation of long-range near-side angular correlations in proton-lead collisions at the LHC*. Phys. Lett. B **718** (2013), 795.
3. S. CHATRCHYAN *et al.*, CMS Collaboration: *Observation of long-range near-side angular correlations in proton-proton collisions at the LHC*. JHEP **1009** (2010), 091.
4. S. CHATRCHYAN *et al.*, CMS Collaboration: *The CMS experiment at the CERN LHC*. JINST **03** (2008), S08004.
5. S. CHATRCHYAN *et al.*, CMS Collaboration: *Multiplicity and transverse-momentum dependence of two- and four-particle correlations in pPb and PbPb collisions*. Phys. Lett. B. **724** (2013), 213.
6. P. BOZEK: *Collective flow in p-Pb and d-Pd collisions at TeV energies*. Phys. Rev. C **85** (2012), 014911.
7. A. BILANDZIC, R. SNELLINGS and S. VOLOSHIN: *Flow analysis with cumulants: Direct calculations*. Phys. Rev. C **83** (2011), 044913.
8. S. VOLOSHIN and Y. ZHANG: *Flow study in relativistic nuclear collisions by Fourier expansion of azimuthal particle distributions*. Z. Phys. C **70** (1996), 665.
9. K. DUSLING and R. VENUGOPALAN: *Explanation of systematics of CMS p+Pb high multiplicity di-hadron data at $\sqrt{s_{NN}}=5.02$ TeV*. Phys. Rev. D **87** (2013), 054014.
10. K. DUSLING and R. VENUGOPALAN: *Evidence for BFKL and saturation dynamics from di-hadron spectra at the LHC*. Phys. Rev. D **87** (2013), 051502.
11. K. DUSLING and R. VENUGOPALAN: *Comparison of the Color Glass Condensate to di-hadron correlations in proton-proton and proton-nucleus collisions*. Phys. Rev. D **87** (2013), 094034.
12. B. ABELEV *et al.*, ALICE Collaboration: *Long-range angular correlations on the near and away side in pPb collisions at $\sqrt{s_{NN}}=5.02$ TeV*. Phys. Lett. B **719** (2013), 29.
13. G. AAD *et al.*, ATLAS Collaboration: *Measurement with the ATLAS detector of multi-particle azimuthal correlations in p + Pb collisions at $\sqrt{s_{NN}}=5.02$ TeV*. arXiv:1303.2084, Phys. Lett. B (2013), submitted for publication.
14. J.-Y. OLLITRAULT, A.M. POSKANZER and S.A. VOLOSHIN: *Effect of flow fluctuations and nonflow on elliptic flow methods*. Phys. Rev. C **80** (2009), 014904.
15. B. ALVER *et al.*, PHOBOS Collaboration: *Event-by-event fluctuations of azimuthal particle anisotropy in Au + Au Collisions at $\sqrt{s_{NN}}=200$ GeV*. Phys. Rev. Lett. **104** (2010) 142301.

Jovan Z. Milošević
 Vinča Institute of Nuclear Science
 University of Belgrade
 Mike Petrovića Alasa, 12-14
 P. O. Box 522
 11001 Belgrade, Serbia
 jovan.milosevic@cern.ch